arXiv:cond-mat/0409711v1 [cond-mat.str-el] 28 Sep 2004

# Ground state of a two dimensional quasiperiodic quantum antiferromagnet

A. Jagannathan
*Laboratoire de Physique des Solides,*
*Université Paris-Sud, 91405 Orsay, France*

(Dated: February 2, 2008)

We consider the antiferromagnetic spin-1/2 Heisenberg model on a two-dimensional bipartite quasiperiodic tiling. The broken symmetry ground state in this model is inhomogeneous, but nevertheless bears interesting similarities with that of the square lattice antiferromagnet. An approximate block spin renormalization scheme developed first for the square lattice is generalized here to the quasiperiodic case. The ground state energy and local staggered magnetizations for this system are calculated, and compared with the results of a Quantum Monte Carlo calculation for the tiling.

PACS numbers: PACS numbers: 75.10.Jm, 71.23.Ft, 71.27.+a

## I. THE EXPERIMENTAL AND THEORETICAL BACKGROUND

Magnetism in quasicrystals can be very complex, due to the extreme sensitivity to structural details, in such systems, of local moment amplitudes as well as of the interactions. A considerable simplification of the problem is however possible for the recently studied rare-earth based quasiperiodic alloy ZnMgHo [1]. The rare-earth based magnetic alloys represents a conceptually simpler system than the transition metal alloy quasicrystals that were initially the object of experimental studies, since the magnetic moments are associated with f-orbitals, and can be assumed in the first approximation to be *independent* of the local itinerant-electron density of states.

This is to be contrasted with the earliest magnetic quasicrystals of the AlMn family, where the itinerant magnetic moments on the Mn atoms depend sensitively on detailed structural features due to the d-orbital hybridization (see the review by Hippert et al in [2]). To add to the difficulties the early alloys were metastable quasicrystals of inferior structural quality so that the role of disorder had to be considered in addition to the intrinsic behavior. Experimental results indicated a wide distribution of effective moments on the Mn atoms, as well as of the interactions between these, leading to a large number of unknown parameters in the phenomenological models describing such systems. From a theoretical viewpoint, therefore, the rare earth system is clearly far simpler.

ZnMgHo was shown to undergo a magnetic transition into a magnetic state characterized by short range antiferromagnetic correlations with quasiperiodic modulation [1]. The experimental results lead naturally to the question of what properties one expects for the ground state of a quasicrystal with short range antiferromagnetic interactions. An acceptable starting point for models of such systems could be, as for crystalline compounds, a Hamiltonian with short range antiferromagnetic couplings between pairs of identical spins, $H = \sum J_{ij}\mathbf{S}_i.\mathbf{S_j}$.

Fig.1 shows the results of a recent Monte Carlo study of a two-dimensional model of quantum spins on a quasiperiodic tiling [3]. The circles on the vertices have radii that depend on the value of the local staggered moment, a quantity that we will define further below. The tiling considered is the eight-fold symmetric octagonal (Ammann-Beenker) tiling, in which sites can have six possible values of coordination number $z$. Sites were occupied by $S = \frac{1}{2}$ spins, with uniform interactions $J_{i,j} = J > 0$ along the edges of the tiling. The system is bipartite, meaning that every spin belongs to one of two sublattices and interactions couple only spins of different sublattices. Analogously to the spin $\frac{1}{2}$ square lattice antiferromagnet, which is now believed to have a ground state with long range order, we expect that this quasiperiodic system, too, has a broken symmetry ground state with long range order. Classically, the ground state corresponds to having oppositely directed sublattice magnetizations, with no frustration, in the sense that all bonds can be "satisfied" simultaneously. In the quantum case, the ground state will correspond to zero total spin since for the octagonal tiling, the two sublattices are equiva-

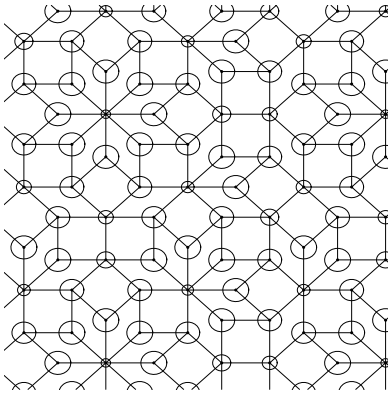

FIG. 1: Inhomogeneous ground state structure on the tiling. The circles have sizes that depend on the strength of the local order parameter

lent.

The inhomogeneous structure of the ground state seen in Fig.1 is a reflection of the environment-dependence of the quantum fluctuations around the Neel state in the quasicrystal. There is for the moment no spin wave expansion that would allow, as in a periodic solid, to calculate the distribution of staggered moments and explain the QMC results. In fact, as we will see, a real space approach seems more appropriate for quasiperiodic tilings, and many such calculations exist for the case of one dimension.

One-dimensional models to study the behavior of quantum spins on quasiperiodic chains been considered by several authors. Quantum spin chains have been analyzed using renormalization schemes [4, 5] based on the inflation symmetry of these chains. Using a mapping to fermionic models and techniques of bosonization, [6] it is possible to obtain interesting results concerning global properties such as the magnetization as a function of external field, and the spectral gaps for a variety of different quasiperiodic sequences. However, real space information such as the distribution of the local quantities $m^2_{loc,i} \sim |\langle S_i S_{i+1} \rangle|$ has not so far been calculated.

For two dimensional structures, real space configurations have been studied for models with classical spins. Here, the ground state is nontrivial only when the model includes frustration. In [7] Godreche et al introduced a renormalization scheme on the Penrose tiling for a Heisenberg exchange model with competing antiferromagnetic interactions, and were thus able to obtain a phase diagram consisting of a variety of ordered phases. The real space spin configurations were calculated numerically in [8] for classical spins interacting via long-ranged dipolar interactions, and a complex magnetization distribution with overlapping decagonal rings reflecting the underlying Penrose tiling was found. A quasiperiodic magnetic state with a heirarchical ringed structure was found, as well, in a different context: that of itinerant magnetism due to interacting electrons [9].

With this background, we return to the problem of quantum Heisenberg spins with nearest neighbor antiferromagnetic interactions. Ref. [3] presented local staggered order parameters similar to the quantities $m_{loc,i}$ above, calculated for individual sites using the expectation values for local spin-spin correlations. One sees in Fig. 1 that sites of the same $z$ have similar local order parameter amplitudes. An explanation of this behavior was given by considering isolated star shaped clusters called Heisenberg stars in [3]. This provided a qualitative understanding of the decrease of local staggered magnetizations as a function of $z$, but for a more quantitative fit to the QMC results, it is necessary to go beyond the isolated cluster approximation, and take into account longer range correlations. This can be done in a renormalization group (RG) calculation that uses an important symmetry of the tiling, namely invariance under discrete scale transformations called inflations. This renormalization group is a generalization of the calculation of Sierra and Martin-Delgado for the square lattice [10], where the authors considered star-shaped block spins formed by a central spin and its four nearest neighbors. In their calculation, block spins formed from these five-spin clusters are shown to interact via an effective Heisenberg antiferromagnetic interaction on a bigger $\sqrt{5} \times \sqrt{5}$ square lattice. The effective spin values scale to infinity, i.e. the classical limit, under renormalization. Their model for a translationally invariant system can, as we will see, be adapted to our quasiperiodic case under certain approximations. We thus calculate not only the global ground state energy as was done for the square lattice, but also the distribution of local order parameters. We will discuss the method, which has been briefly reported in [11], in some detail in the present paper.

We begin with an introduction to the quasiperiodic tiling and the spin Hamiltonian in the next two sections. The RG scheme is described in the fourth section. Results and discussions are presented in sections five and six.

## II. REVIEW OF GEOMETRICAL ASPECTS

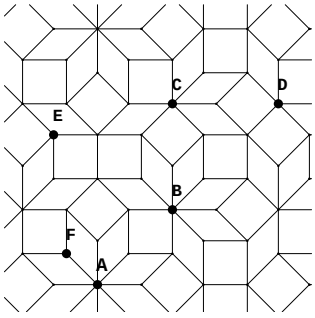


FIG. 2: A portion of the octagonal tiling showing the six different nearest neighbor environments A,B,...,F

### 1. Some general remarks

The octagonal tiling [12] shown in Fig.2 can be thought of as the equivalent of the square lattice for quasiperiodic systems. It has therefore been frequently used for analytical and numerical investigations of the effects of quasiperiodic modulations in two dimensions. Spectral properties of electrons [13], transport properties [14], vibrational properties [15] and magnetic properties [3] have thus been studied for discrete models defined on the octagonal tiling. The tiling is built from two kinds of tiles, squares and $45^o$ rhombuses. These two types of tiles can

fill the two-dimensional plane in an aperiodic way, as Penrose first showed for the five-fold tiling named after him [16, 17].

Although there is no translational invariance in a quasiperiodic tiling, any given tile arrangement of tiles reoccurs all over the tiling with a certain frequency of re-occurrence – or, alternatively viewed, there exists a mean distance of separation between such identical domains. This is referred to as the repetitivity property of quasiperiodic tilings, and is very different from the situation in a disordered medium (where the expected distance in which one expects to find a second region identical to the first increases exponentially with the size of the region). Similarly, the property of symmetry under rotations for these tilings differs from that in crystals, for which the new and the old structures coincide exactly. For the quasicrystal, the equivalence of the new and old tilings holds in the "weak" sense, namely, any finite region of the new tiling after rotation will be identical to finite regions of the old one.

Such aperiodic structures can be built using "matching rules". These are local rules that determine if and how two tiles can be laid side by side (see Ch.1 of [18]). Alternatively, tilings such as the Penrose and octagonal tilings could be generated by a projection method down from a higher dimensional periodic structure [19]. Such an approach can give either a deterministic, perfectly ordered tiling, or a random one where tiles are assembled subject only to the constraint that they should fill space without overlapping [20]. Random tilings are of great theoretical interest, but we are here interested in deterministic tilings, which have the important property of invariance under inflation/deflations, or discrete scale invariance. This symmetry is illustrated in Fig. 3 and will be described in more detail in the next section. It is this property that is responsible for the characteristic singular electronic and magnetic properties of such tilings and it was first pointed out in the Penrose tiling, which is invariant under a replacement of tiles by $\tau$-fold bigger tiles, where $\tau = (\sqrt{5}+1)/2$ [17]. One can define geometrical inflation rules for, among others, the Fibonacci chain in one dimension, the octagonal tiling in two dimensions, and the icosahedral tiling in three dimensions.

The renormalization approach is a natural one for such geometrically self-similar quasiperiodic tilings , and this structural property has been exploited in order to establish recurrence relations for parameters occurring in discrete spin models, electron hopping models, etc, as mentioned before for the one-dimensional case, but also for some two-dimensional models [7, 21], where analytical methods remain hard to implement. As noted in the introduction, our approach is inspired by the renormalization calculation of Sierra and Martin-Delgado [10] for the square lattice.

Some principal properties of the octagonal tiling that are used in the RG calculation are reviewed in the next section, without demonstration. (For those interested, Appendix A contains some additional details on how to obtain a quasiperiodic structure, and how inflations/deflations are described in the framework of the projection method. Although not strictly necessary to understand the calculations presented below, an understanding of the geometrical properties of the tiling is important for those wishing to improve this approximate RG scheme and extend it to other models. For more details, the reader is referred to reviews in [22, 23]).

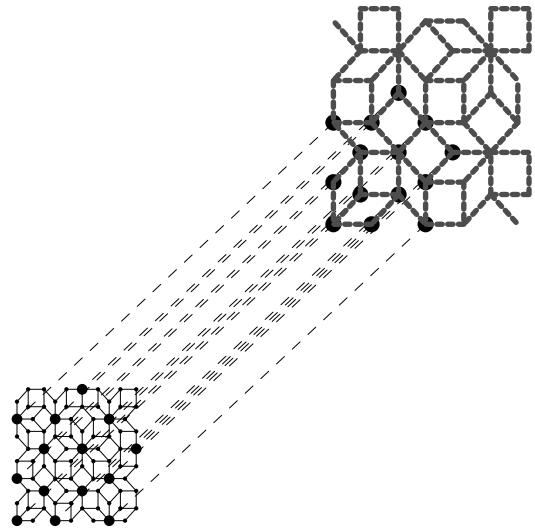

FIG. 3: Portion of original (black) tiling, showing sites of the $\alpha$ class (black dots) which become sites of the new inflated (grey) tiling

### 2. The six local environments

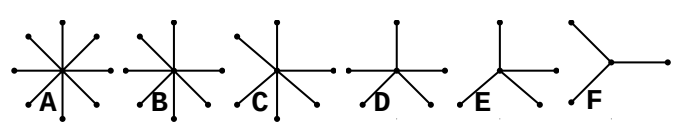


FIG. 4: The six different nearest neighbor environments of the octagonal tiling

The six nearest neighbor configurations, corresponding to coordination numbers $z = 8, 7, ..., 3$ are labeled A,B,...,F as shown in Fig.2. Fig. 4 shows these environments separately. In an infinite tiling, each of these types of site occurs with a well-defined frequency $f_i$, where (see Appendix A)

$$f_A = \lambda^{-4}; f_B = \lambda^{-5}; f_C = 2\lambda^{-4};$$

$$f_{D1} = \lambda^{-3} = f_{D2}; f_E = 2\lambda^{-2}; f_F = \lambda^{-2} \quad (1)$$

with $\lambda = 1 + \sqrt{2}$. One distinguishes between two kinds of D sites as explained in the next section. It can be checked using the above frequencies that the average site coordination number on the octagonal tiling is exactly four.

### 3. The inflation transformation

Inflation proceeds as follows for the octagonal tiling: one starts with a tiling composed of tiles of a given initial edge length (we will assume this is equal to 1) and one reconnects a precisely determined subset of vertices so as to obtain a new tiling of the same type as the old, i.e. having the same set of local geometries, except for an overall scale change by a numerical factor $\lambda = 1 + \sqrt{2}$ ( Fig.4). The sites shown as black dots on the original tiling belong in the $\alpha$ class: A,B,C and half the D (called $D_1$) sites. These become the sites of the new bigger tiling, while the remaining ($\beta$) sites drop out. Note that there are two varieties of five-fold sites, $D_1$ and $D_2$, which belong to the $\alpha$ and $\beta$ classes respectively. On the octagonal tiling, they always occur in pairs. Appendix A shows how the two classes of D sites can be distinguished in terms of their perpendicular space coordinates [24].

Under inflation, the density of sites is reduced to $1/\lambda^2$ of its initial value. The sites that remain acquire new values of the site coordination numbers $z' \leq z$. The table below lists the initial and final values of coordination number for each of the $\alpha$ class sites (note that there are four different subcategories for the A sites – see Appendix A for more on the properties of these subcategories).

| initial site (z value ) | | final site (z value) |
|---|---|---|
| A (8) | → | A,B,C or $D_1$ (8,7,6,5) |
| B (7) | → | $D_2$ (5) |
| C (6) | → | E (4) |
| $D_1$ (5) | → | F (3) |

Table 1. List of $\alpha$ sites and their transformations under inflation

### 4. Nearest neighbors of $\alpha$ sites

For the four types of $\alpha$ sites, the table below lists the nearest neighbors (nn) in terms of the type of site and the number of sites of that type. This information will be useful in determining the final block spin value at the central site, as we will explain in sec.III.

| $\alpha$ site | nn spin type(number) |
|---|---|
| A | F (eight) |
| B | F (five), E (two) |
| C | F (two), E (four) |
| $D_1$ | $D_2$ (one),E (four) |

Table 2. The $\alpha$ sites and their nearest neighbor environments

Table 2, in conjunction with Table 1 allows one to deduce how blocks are organized in the tiling. An A site which transforms to an A site after inflation corresponds, on the original tiling to an A block surrounded by eight $D_1$ blocks.

## III. THE SPIN HAMILTONIAN

We consider onsite spins $\mathbf{S_i}$ ( i=1,N) where all spins have spin $\frac{1}{2}$, with the Hamiltonian $H(N, \{S_i\}, \{J_{ij}\})$

$$H = \sum_{\langle i,j \rangle} J_{ij} \mathbf{S}_i . \mathbf{S}_j \quad (2)$$

where $\langle i, j \rangle$ denotes a pair of spins $\mathbf{S_i}$ and $\mathbf{S_j}$ linked by an edge, and $J_{ij} = J > 0$ for such a pair. This system is bipartite with two identical (to be understood in the weak sense) subtilings (as on the square lattice).

### 1. Finite spin clusters

A sites are surrounded by eight F sites. If one isolated one such cluster of 8+1 spins, the lowest energy state for classical spins is the one with the eight peripheral spins antiparallel to the central spin. In the quantum case, the ground state of the cluster is rotationally invariant, and corresponds to the total cluster spin value $S_{tot} = 7/2$. The other $\alpha$ sites correspond to total cluster spin values in the ground state of $S_{tot} = (z_B - 1)/2 = 3$ around a B site, and so on. The four clusters are shown in the left hand side series of Fig.5.

Clusters of each type can be defined on larger and larger length scales, by using the inflation rules already outlined to determine the new A,B,C and $D_1$ sites after inflation. Fig.5 shows the four $\alpha$ clusters on the next largest length scale on the right hand side series. Here, block spin centers are shown with big black dots, while the sites corresponding to the $\beta$ sites are indicated by smaller dots. On a yet bigger length scale, Fig.6 shows a "second generation A site", namely, a site that remains of A type after two inflations, along with all the sites belonging to the cluster before the two decimations.

The $\alpha$ clusters on all length scales are the building blocks for the renormalization scheme that follows.

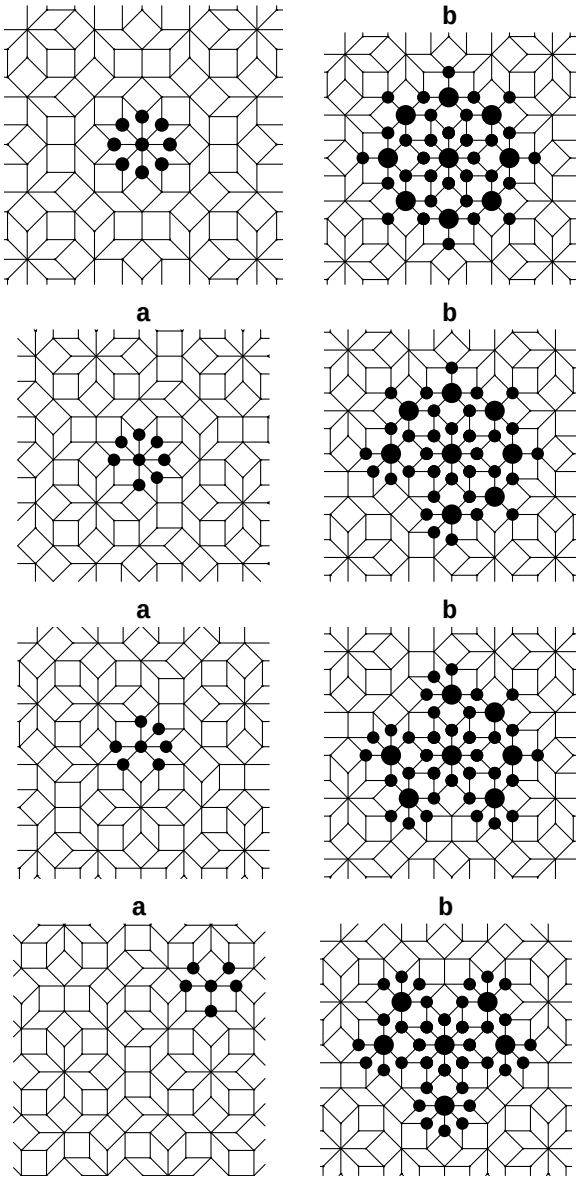


FIG. 5: The $\alpha$ site clusters defined on the original (left) and once inflated (right) tilings

## IV. THE RENORMALIZATION TRANSFORMATION

The renormalization calculation is a generalization to an aperiodic system of the one used for the square lattice by Sierra and Martin-Delgado [10]. We review briefly the steps of their calculation before showing how they are modified in the quasiperiodic case.

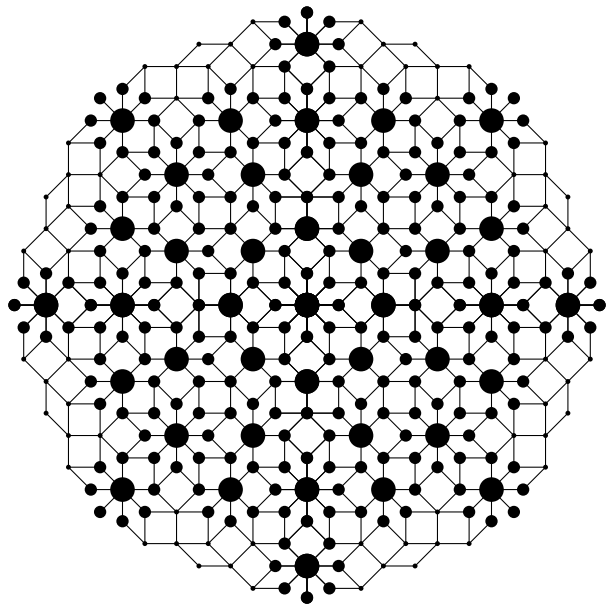

FIG. 6: Second generation A cluster

### 1. RG on the square lattice

We consider the nearest neighbor Heisenberg antiferromagnet described by Eq. 2 with spin $\frac{1}{2}$ on the vertices and the initial coupling $J$ along the edges of the squares (of side $a = 1$). Fig.7 shows the five-spin blocks enclosed by circles. The four couplings inside each block are shown outlined by thick grey lines. As one sees, the block spins form a new rotated square lattice of side $\sqrt{5}$ (Fig.7). Each of the blocks can be diagonalized exactly. With every step of RG, only the lowest energy states of the blocks are retained to form the basis for the effective Hamiltonian. $T_0$ and $T_0^\dagger$ denote the operators describing the transformations from the original Hamiltonian (acting in the complete Hilbert space) to the effective Hamiltonian (acting in the reduced Hilbert space). For a single block, the lowest energy sector corresponds to spin $\frac{3}{2}$, and the ground state energy is $e_0 = -JS(4S+1)$. The couplings not already taken into account give rise to inter-block interactions, calculated by first order perturbation theory. It is easy to check that the new block spins will be coupled antiferromagnetically to its nearest neighbors, like the original spins. The effective Hamiltonian $H(N, S, J)$ can thus be written approximately as a sum of single-block contributions (the diagonal terms) and a set of terms involving nearest neighbor blocks (off-diagonal terms), and the formal expression for the transformed problem reads

$$T_0^\dagger H(N, S, J) T_0 = N' e_0(J, S) + H'(N', S', J') \tag{3}$$

where the new Hamiltonian $H'$ has the same form (bilinear in $S'$) as $H$, and $N' = N/5$. The effective spin of a block spin is $S' = 3S = \frac{3}{2}$ . The spin renormalization factor relating one of the four boundary spins to the new block spin has been shown to be close to the classical value $\xi_0 = S_i/S' \approx \frac{1}{3}$ ( see [10] for the exact value). The interaction between two contiguous blocks is $J' = 3\xi_0^2 J$.

Repeating the steps of renormalization, one has ultimately for the ground state energy per site an infinite sum as follows

$$e_\infty = -\frac{1}{5}\sum_{n=0}^{\infty} 5^{-n} J^{(n)} S^{(n)}(4 \times 3^n S + 1) \qquad (4)$$

where $S^{(n+1)} = 3S^{(n)}$ and $J^{(n+1)} = 3\xi^2(S^{(n)})J^{(n)}$. Under RG, the spins evolve to the classical limit, $S \to \infty$ indicating that in the quantum case as well one has a ground state with broken symmetry. The couplings scale to zero indicating the model is massless. Qualitatively, thus, the RG gives the now accepted physics of the model, however, quantitatively the value obtained for $e_\infty \approx -0.546$ is not as good as that obtained by spin wave expansion and is about 15 % higher than that established by numerical calculations [25]. We will return to this point at the end of the paper.

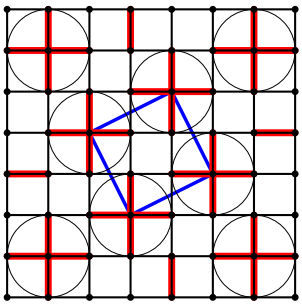

FIG. 7: Five-spin units (surrounded by circles) on the square lattice. The new $\sqrt{5} \times \sqrt{5}$ unit cell is shown

### 2. RG on the octagonal tiling

On the octagonal tiling, it is clear that several kinds of block spins must be introduced. A natural choice is to designate the $\alpha$ sites as block spin centers. Fig.12 shows the positions of the block spins (black dots) on a portion of the tiling. Upon inflation, the other sites will disappear, leaving only the block variables, and some residual interactions between them. If no new couplings are generated, one will find an effective Hamiltonian similar to the old, except for the renormalized couplings which become site dependent. One can repeat the process, and determine if there is convergence to a fixed point.

The simple scheme outlined above cannot be implemented without some modifications and approximations. The first problem arises because the connectivity of the tiling is such that some of the block spins overlap, that is, share two intermediate $\beta$ sites in common. This is shown by the thick grey lines in Fig.12, which indicate the boundary between overlapping blocks. Overlapping occurs between contiguous $C$ and $D_1$ blocks, as well as between contiguous $D_1$ blocks. This overlapping occurs with a finite density. One can calculate this density by noting that the shared sites occur between any two sites that are a distance $\lambda^2 d_s$ apart, where $d_s$ is the short diagonal of the rhombus. One finds, using the relative frequencies of occurrence of squares and rhombuses that the density of pairs is $\sqrt{2}/\lambda^3$, that is, about 10% of the total number of pairs.

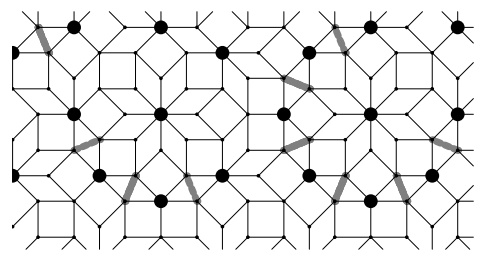

FIG. 8: Tiling showing block centers (black dots). The grey lines connect pairs of sites that are shared between two blocks.

To deal with this problem, we therefore considered two possible modifications of the original model, i) doubling the number of spins on each shared site, and considering each spin as being coupled to one block only, and ii) decoupling the block spins by annulling one of the bonds to the left or the right so that spins are no longer coupled on both sides. The first modification leads to overestimating the total energy, the second to underestimating it, with respect to the original octagonal tiling. Spin doubling on selected sites leads to an uninteresting flow under renormalization, where cluster energies basically repeat a scaled Heisenberg star distribution at each step. The bond dilution scheme yields a more complicated behavior of cluster energies under renormalization, and is the option taken up in detail in this paper.

We note that the diluted model remains two-dimensional, and is not of a scale invariant fractal such as the Sierpinski gasket [26], where bonds are also deleted heirarchically but in a way that leads to an effective fractal dimension less than two.

The second problem is the quasiperiodic connectivity between blocks which leads ultimately to an infinite number of environments. This is dealt with by truncating

the number of environments we choose to distinguish between. The $\alpha$ sites always have the same type of nearest neighbors (given in Table 2), however the $\beta$ sites occur in several configurations. We will now truncate the table of connectivities by allowing only one type of $D_2$,E and F site, and a connectivity table as follows:

| $\beta$ site | nn spin type(number) |
|---|---|
| $D_2$ | $D_1$ (one),E (two),F(two) |
| E | $\alpha$ (two), F (two) |
| F | $\alpha$(one), E (two) |

Table 3. The $\beta$ sites and the truncated set of nearest neighbor environments

### *A. Bond dilution and the new block spins*

In this subsection we discuss the blocks that are obtained after dilution and the values of the effective block spin. Fig.9(top) shows in detail a central $D_1$ site which transforms to an F site under inflation. The three neighboring block spins are shown as well, with the block spin sites shown by black dots. The original links are indicated by thin black lines, while the new effective links on the inflated tiling are shown by thick grey lines. Fig.9(middle) shows a C site transforming to an E site, with the same conventions used to denote block spin sites and new effective couplings. In this figure one sees that two of the block spins, corresponding to neighboring $D_1$ blocks, overlap. The pair of sites shared between the two blocks is coupled to the left and right by a total of four bonds. In the bond-dilution approach, one has to set two of the bonds equal to zero. This can be done in one of two ways that treat the two blocks equitably, leaving each $D_1$ block with one less bond. Finally, Fig.9(bottom) shows an A site transformed under inflation to a final A site. In this case, the eight $D_1$ blocks surrounding the center block form a ring of overlapping blocks. There are two ways to decouple them all by annulling eight of the sixteen links joining them in way that treats all the $D_1$ sites equitably. Ultimately, the bond dilution results in an effective reduction of connectivity of C and $D_1$ sites: the former have the effective $z$ value $\tilde{z} = 5$ and the latter $\tilde{z} = 3$.

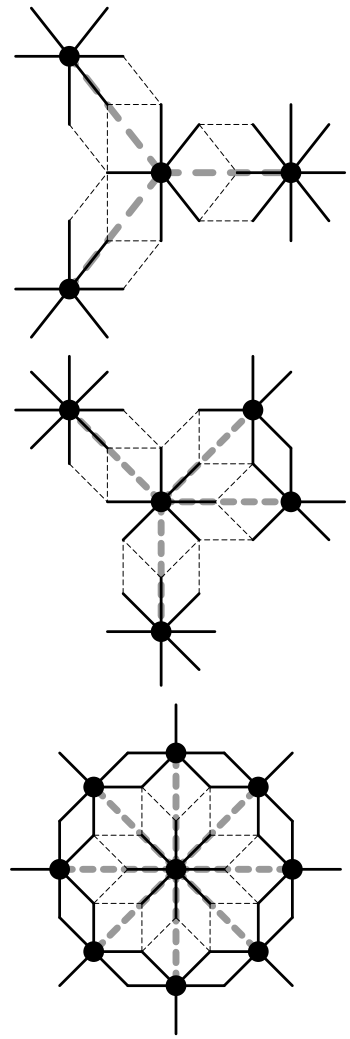

FIG. 9: Block spin centers (filled circles) showing the central and all peripheral blocks for three cases: (top) a $z = 5, z' = 3$ site (middle) a $z = 6, z' = 4$ site (bottom) a $z = z' = 8$ site

### *B. Spin renormalization factors*

Consider a block spin composed from a cluster of $z$ spins surrounding a central spin and antiferromagnetic interactions. In the simplest case where all spins have the value S, the block has a spin of $S' = (z-1)S$ in the ground state. The spin renormalization factors are taken to be equal to the classical value for simplicity, so that for a given block $\xi_z = (z-1)^{-1}$. The new block spins $S'$ are situated on the black circles representing the sites of the inflated lattice, while all of the nearest neighbors are decimated in the renormalization group (RG) transformation. Initially, all spins have the same value of spin, $s_0 = \frac{1}{2}$, so that after one inflation the block spin variables are simply $\mathbf{S}^{(1)} = \{S_A^{(1)}, ....., S_F^{(1)}\} = \{7s_0, 7s_0, 7s_0, 7s_0, 6s_0, 4s_0, 2s_0\}$. (Note that for $E$ and $F$ sites, the value of z was corrected for the bond dilution). In subsequent inflations, one has the following matrix relation $\mathbf{S}^{(n)} = (S_A^{(n)}, ..., S_F^{(n)}) = C\mathbf{S}^{(n-1)}$, with

$$C = \begin{pmatrix} -1 & 0 & 0 & 0 & 0 & 0 & 8 \\ -1 & 0 & 0 & 0 & 0 & 0 & 8 \\ -1 & 0 & 0 & 0 & 0 & 0 & 8 \\ -1 & 0 & 0 & 0 & 0 & 0 & 8 \\ 0 & -1 & 0 & 0 & 0 & 2 & 5 \\ 0 & 0 & -1 & 0 & 0 & 3 & 2 \\ 0 & 0 & 0 & -1 & 1 & 2 & 0 \end{pmatrix} \tag{5}$$

Note that the number of values of the block spins after each inflation does not grow – there are just four possible different values of the block spin at any stage of inflation. As in the square lattice example, the spins all tend to the classical limit as $n$ goes to infinity. In addition, the largest eigenvalue of $C$, 3, is precisely that of the square lattice in section IV.1 ! This eigenvalue, along with the corresponding eigenvector gives the flow of effective spin values in the limit of large $n$. Thus for large $n$ $\mathbf{S}^{(n)} \approx 3\mathbf{S}^{(n-1)}$. This is the same spin renormalization as that on the square lattice where $z$ is everywhere equal to 4. In both cases, the spins tend to infinity, i.e. the classical limit, under renormalization. On the tiling, moreover, the block spins tend to constant relative asymptotic values which are site dependent and given by the eigenvector $(1, 1, 1, 1, 1, \frac{3}{4}, \frac{1}{2})$.

### C. Ground state energy of an isolated block

Consider the configuration of $z + 1$ spins of Fig.10 in which each of the $z$ links represent the same antiferromagnetic coupling $J$, termed the Heisenberg Star (HS) in [3]. For spin $\frac{1}{2}$ variables on each site and for a given antiferromagnetic coupling J between the central spin and its $z$ neighbors, the ground state energy can be found exactly to be

$$\epsilon^{(0)}(z) = -J(z + 2)/4 \tag{6}$$

On the octagonal tiling, one has the seven different families of star clusters on the tiling, with the corresponding values of $z$ on the right hand side of the equation. The superscript "0" indicates that this corresponds to the energy of unrenormalized clusters. We also require the ground state energy in the case of clusters of spins of unequal lengths. The lowest energy state of a cluster in which $z$ spins of unequal lengths $S_i = n_i s_0$ are coupled with strength J to a central spin $S_0 = n_0 s_0$ is taken to be the following generalisation of Eq.6

$$\epsilon(J, z, \{n\}) = -n_0 J(\sum_{i=1}^{z} n_i + 2)/4 \tag{7}$$

In the present model, although initially the couplings are all equal, after one RG step the couplings take on different values. Therefore we shall make an approximation later that consists of replacing the set of couplings around each site by a single locally averaged value.

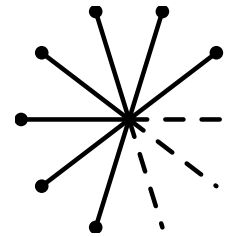

FIG. 10: ($z$+1) spin cluster (Heisenberg Star)

### D. Proliferation of blocks under deflation

If $\mathbf{n} = (n_A, n_B, n_C, n_{D1})$ are the number of blocks in a given region of each given type, the number of blocks of each type after one deflation is $P\mathbf{n}$ where

$$P = \begin{pmatrix} 1 & 0 & 0 & 8 \\ 1 & 0 & 2 & 5 \\ 1 & 0 & 4 & 2 \\ 1 & 1 & 4 & 0 \end{pmatrix} \tag{8}$$

The largest eigenvalue of the proliferation matrix $P$ is equal to 7 so that the total number of blocks increases(decreases) with the number $m$ of deflations(inflations) as $7^m$ for large $m$. Notice that the proliferation of blocks is described by an integer, and not the irrational number $\lambda^2 \approx 6.8$, each of these numbers being the answer to a different question. The former describes the rate of growth of a finite system in terms of the number of blocks. The latter is the scale factor of the change of site density under inflation/deflation for the infinite quasicrystal, and this is not restricted to have integer values.

### E. Renormalization of links

There are an infinite number of types of links since each link couples two sites that are each unique. However, just as we chose to truncate the size of the space of solutions by distinguishing only seven types of sites, we can consider a "minimal" model where it suffices to take into account only five kinds of links. These are represented in an array $\mathbf{j} = (j_{\alpha F}, j_{\alpha E}, j_{D_1 D_2}, j_{D_2 F}, j_{EF})$. Here, $j_{\alpha F}$ is used to denote the link between (A,F), (B,F),(C,F) and ($D_1$,F) pairs. Similarly, $j_{\alpha E}$ denotes the link connecting (B,E),(C,E) and ($D_1$,E) pairs. This oversimplification of the link classification ignores, in particular, that E and

F sites can occur in more than one environment. However, in the first approximation, we have assumed here that one can treat all the sites of a given family as identical out to first neighbors, and this approximation will be found *post facto* to yield reasonably good numerical results.

Note that there are no bonds linking sites that are separated by a distance $d_s$ in the original tiling (recall that this is the shortest distance possible on the octagonal tiling) and the same is true for the sites of the inflated tiling since our bond dilution has the effect of decoupling such blocks.

Interblock links are all the links not taken into account in the definition of blocks. To find the new effective links, one also allows for bond moving, as illustrated by the following example: consider a central A site surrounded by eight $D_1$-clusters. These transform to an A site with eight F sites around it after an inflation. We wish to obtain the effective link between the central A and one of the F sites. The original A site has sixteen links to the eight $D_1$-clusters - i.e. it has two links per $D_1$-cluster. These two links between the center and each peripheral block are of the $EF$ type (see Fig.8c). Thus the new effective coupling between the central $A \to A$ site and each of the eight $D_1 \to F$ sites around it on the inflated tiling is of the $\alpha F$ type. It is antiferromagnetic, like the original couplings. One takes into account the spin renormalization factors of the block spins mentioned before, namely $\xi_A$ and $\xi_D$ respectively. The new coupling can then be expressed in terms of the previous generation of couplings by the equation

$$j^{(1)}_{\alpha F} = 2 j^{(0)}_{EF} \xi^{(0)}_A \xi^{(0)}_D \tag{9}$$

For the second type of links, $j_{\alpha E}$ , one sees that there are three $EF$ links joining a $A \to B$ site to a $C \to E$ site, so that the new $\alpha E$ link is given by

$$j^{(1)}_{\alpha E} = 3 j^{(0)}_{EF} \xi^{(0)}_A \xi^{(0)}_C \tag{10}$$

The other effective couplings can be written down similarly, although a problem arises due to the fact already mentioned, namely, that E and F sites can occur in more than one local environment. Here we chose just one option among the several, to write down the new effective $D_2F$ and $EF$ couplings. With this truncation of the link relations, we have a system of equations between the five old and five new couplings, $\mathbf{j}^{(1)} = M^{(0)}\mathbf{j}^{(0)}$, where

$$M^{(n)} = \begin{pmatrix} 0 & 0 & 0 & 0 & 2\xi^{(n)}_A \xi^{(n)}_D \\ 0 & 0 & 0 & 0 & 3\xi^{(n)}_A \xi^{(n)}_C \\ 0 & 0 & 0 & 0 & 4\xi^{(n)}_A \xi^{(n)}_B \\ 0 & \xi^{(n)}_B \xi^{(n)}_D & 0 & \xi^{(n)}_B \xi^{(n)}_D & \xi^{(n)}_B \xi^{(n)}_D \\ 0 & \xi^{(n)}_C \xi^{(n)}_D & 0 & \xi^{(n)}_C \xi^{(n)}_D & \xi^{(n)}_C \xi^{(n)}_D \end{pmatrix} \tag{11}$$

with the initial condition (taking the zero order coupling $J = 1$) $\mathbf{j}^{(0)} = (1, 1, 1, 1, 1)$.

### *F. Averaged values of renormalized couplings*

After one inflation, the new tiling has the same geometry, with the same relative frequencies of vertices as the old tiling, however, the new onsite spins $\mathbf{S^{(1)}}$ and intersite couplings $\mathbf{j}^{(1)}$ are no longer uniform from site to site. To proceed, we define averaged quantities – averaged renormalization factors $\xi^{(1)}_i$ and averaged couplings, for each of the seven types of site. The average couplings are easily found, using the local environments listed for each of the seven families in Tables 2 and 3. The simplest situation occurs for $A$ sites, which have eight A-F links surrounding them, so that the average coupling is just $\overline{\jmath}^{(n)}_A = j^{(n)}_{\alpha F}$. For the six remaining sites we can similarly define averaged couplings that are linear combinations of the $j^{(n)}$. Dropping the superscripts, we thus have seven averaged couplings as follows:

$$\begin{aligned} \overline{\jmath}_A &= j_{\alpha F} \\ \overline{\jmath}_B &= (5 j_{\alpha F} + 2 j_{\alpha E})/7 \\ \overline{\jmath}_C &= (2 j_{\alpha F} + 3 j_{\alpha E})/5 \\ \overline{\jmath}_{D_1} &= (2 j_{\alpha E} + j_{DD})/3 \\ \overline{\jmath}_{D_2} &= (2 j_{\alpha E} + 2 j_{DD} + 2 j_{D_2 F})/5 \\ \overline{\jmath}_E &= (2 j_{\alpha E} + 2 j_{EF})/4 \\ \overline{\jmath}_F &= (j_{\alpha F} + 2 j_{EF})/3 \end{aligned} \tag{12}$$

Average renormalization factors $\xi^{(1)}_i$ are analogously determined for each of the seven sites, and used to obtain the new matrix $M^{(1)}$. This process is repeated and the result is a set of recurrence relations $\mathbf{j}^{(n+1)} = M^{(n)}\mathbf{j}^{(n)}$ with $M$ having the same structure as in Eq.8. One can now study the evolution of the matrix $M$ under successive inflations. The maximum eigenvalue of $M$, $\gamma_5 \approx 0.15$. This results in a power law decay of the couplings for large $n$, since $\mathbf{j}^{(n)} \approx \gamma_5 \mathbf{j}^{(n-1)}$. The corresponding eigenvector $|\upsilon_5\rangle$ determines the fixed point relative couplings.

### *G. Hamiltonian of inflated system*

The effective Hamiltonian after a single inflation is now written down much as for the case of the square lattice. After the first renormalization there are block spins at each of the $\alpha$-class sites, whose ground state zero order energies are $\epsilon^{(0)}_i$ and having new interblock links $\mathbf{j}^{(1)}$. $H^{(1)}(N^{(1)}, \{S^{(1)}_i\}, \{\mathbf{j}^{(1)}\})$, where $H^{(1)}$ has the same form as the original Hamiltonian in Eq.2 and $N^{(1)} = \lambda^{-2}N$. The original Hamiltonian is thus decomposed into a set of independent cluster energies and a set of intercluster terms as follows:

$$H = \sum_{j \in \alpha} f_j \epsilon^{(0)}_j + H^{(1)} \tag{13}$$

where $j$ can take on the values A,B,C or $D_1$. The first term is a sum over the energies of Heisenberg stars defined on the four types of blocks $\alpha$, given by Eq.6 or equivalently by Eq.7 with $\epsilon_j^{(0)} \equiv \epsilon(1, z, n_0 = 1, \sum n_i = z)$.

## V. RESULTS

We will discuss the calculation of the local order parameters and then that of the ground state energy.

### 1. Local staggered magnetic moments

The QMC data in [3] give values of local order parameters. These can be defined in terms of the local energies around a site $i$

$$e_i = \frac{1}{2} J \sum_{\delta} \langle \vec{S}_i . \vec{S}_{i+\delta} \rangle, \tag{14}$$

where the sum is over all the nearest neighbors of a given site $i$, and the spin correlations were evaluated in the ground state. We have added a factor $\frac{1}{2}$ per bond (that is, the bond energy is shared equally between the two sites at each end). The local order parameters are defined by [28]

$$m_{loc,s}^{num} = \sqrt{e_i/z} \tag{15}$$

It is the quantity $e_i$ that we now wish to calculate.

The inflation symmetry of the quasiperiodic system allows us to define clusters on length scales that increase as powers of $\lambda^2$. We would like a relation between the local energies $e_i$ and the cluster energies, denoted $E^{(n)}(z)$, evaluated as a function of $z$ for bigger and bigger cluster size as $n$ increases. The energy *per site* for a cluster of the $i$th type tends to a certain value in the infinite size limit. We propose that this limiting value coincides with the local energies calculated by the QMC. This is based on the expectation that there is a fixed point distribution for cluster energies, like the one found for the block spins, and for the averaged couplings.

The number of terms contributing to the cluster energy is governed by the largest eigenvalue of the block proliferation matrix $P$, so that $E^{(n)}/7^n$ tends to a limit as $n \to \infty$. It is this quantity that corresponds to the numerically evaluated local energies. With this assumption, the local order parameters at every stage of RG are found from

$$m_{loc,s}^{(n)} = \sqrt{\frac{E^{(n)}(z)}{7^n z}}. \tag{16}$$

We now describe how to calculate the cluster energies at each stage of RG.

*Zeroth order calculation*

The zeroth approximation was obtained in [3], the energies of the clusters at this order being easily calculated using Eq.6 for each of the values of z, $e^{(0)} = \epsilon^{(0)}$. The values obtained are

$$\{e_A^{(0)}, ..., e_F^{(0)}\} = \{\frac{5}{2}, \frac{9}{4}, 2, \frac{7}{4}, \frac{7}{4}, \frac{3}{2}, \frac{5}{4}\} \tag{17}$$

The staggered moments corresponding to these energies are a simple function of $z$

$$\begin{aligned} m_{loc,s}^{(0)}(z) &= \sqrt{\epsilon^{(0)}(z)/z} \\ &= \sqrt{\frac{z+2}{4z}} \end{aligned} \tag{18}$$

This function is plotted in Fig.11a (dashed line). In accord with the qualitative trend of the QMC data, it shows that $m_{loc,s}$ decreases with increasing $z$. With each additional bond, the central spin enters into a resonant state with more and more neighboring spins, with the result that for each individual bond there is less amplitude for formation of a singlet.

### A. First order calculation

The seven averaged couplings at this order have the numerical values

$$\{\bar{\jmath}_A, ..., \bar{\jmath}_F\} = \{0.14, 0.13, 0.12, 0.10, 0.16, 0.24, 0.29\} \tag{19}$$

These averaged couplings are used in the calculation of the ground state energy at each of the new clusters. This is done using Eq.7, along with the block spin values for the center and three surrounding blocks deduced from Eq.5. The first order Heisenberg star energies for each of the seven types of site are thus

$$\begin{pmatrix} \epsilon_A^{(1)} \\ \epsilon_B^{(1)} \\ \epsilon_C^{(1)} \\ \epsilon_{D1}^{(1)} \\ \epsilon_{D2}^{(1)} \\ \epsilon_E^{(1)} \\ \epsilon_F^{(1)} \end{pmatrix} = \begin{pmatrix} \epsilon(\bar{\jmath}_A, 8, \{n_0 = 7, \Sigma n_i = 16\}) \\ \epsilon(\bar{\jmath}_B, 7, \{n_0 = 7, \Sigma n_i = 18\}) \\ \epsilon(\bar{\jmath}_C, 6, \{n_0 = 7, \Sigma n_i = 16\}) \\ \epsilon(\bar{\jmath}_{D1}, 5, \{n_0 = 7, \Sigma n_i = 14\}) \\ \epsilon(\bar{\jmath}_{D2}, 5, \{n_0 = 6, \Sigma n_i = 19\}) \\ \epsilon(\bar{\jmath}_E, 4, \{n_0 = 4, \Sigma n_i = 18\}) \\ \epsilon(\bar{\jmath}_F, 3, \{n_0 = 2, \Sigma n_i = 15\}) \end{pmatrix} \tag{20}$$

The energy of a cluster at first order, denoted $E^{(1)}$, includes this Heisenberg star energy and all zero order diagonal terms of the sites belonging to the cluster. These

first order energies of the clusters can be expressed as follows:

$$E_i^{(1)} = \epsilon_i^{(1)} + \epsilon_{anc(i)}^{(0)} + \frac{1}{2}\sum_{j=1}^{z} \epsilon_{anc(j)}^{(0)} \tag{21}$$

where $j = 1, .., z$ are the nearest neighbor sites of $i$, and $anc(i)$ denotes the ancestor of site $i$. This definition takes into account the first order star cluster energy for the cluster $i$ plus the zero energy term for the center site, plus one-half the zero energy terms for the surrounding sites.

To illustrate with an example: consider an A site on the inflated tiling, with eight nearest neighbor F sites around it. The zero order energy term for an A site is the block spin energy of its ancestor A site, namely, $\epsilon_A^{(0)}$. The zero order energy term for F sites is the energy of their ancestor $D_1$ block spins, $\epsilon_{D1}^{(0)}$. Finally, the Heisenberg Star energy for the A site, and with the first order effective coupling $\bar{\jmath}_A^{(1)}$ is $\epsilon_A^{(1)}$.

Consider another example of an F-site which has three neighbors, say an A site and two E sites. The F site arises from a $D_1$ site. The zero order block energy associated with it is therefore $\epsilon_{D1}^{(0)}$. Similarly, the ancestors of the three neighbors are an A and two C sites. They contribute half their block energies, respectively $\epsilon_A^{(0)}$ and $\epsilon_C^{(0)}$, to the total F-cluster energy. The total energy of the F-cluster is found by adding four zeroth order terms plus the HS energy for F sites, which have a first-order coupling $\bar{\jmath}_F^{(1)}$. Other cluster energies can be similarly obtained, and are listed below.

$$\begin{aligned}
E_A^{(1)} &= \epsilon_A^{(1)} + \epsilon_A^{(0)} + \frac{1}{2}(8\epsilon_{D1}^{(0)}) \\
E_B^{(1)} &= \epsilon_B^{(1)} + \epsilon_A^{(0)} + \frac{1}{2}(2\epsilon_C^{(0)} + 5\epsilon_{D1}^{(0)}) \\
E_C^{(1)} &= \epsilon_C^{(1)} + \epsilon_A^{(0)} + \frac{1}{2}(2\epsilon_{D1}^{(0)} + 4\epsilon_C^{(0)}) \\
E_{D1}^{(1)} &= \epsilon_{D1}^{(1)} + \epsilon_A^{(0)} + \frac{1}{2}(\epsilon_B^{(0)} + 4\epsilon_C^{(0)}) \\
E_{D2}^{(1)} &= \epsilon_{D2}^{(1)} + \epsilon_B^{(0)} + \frac{1}{2}(\epsilon_A^{(0)} + 2\epsilon_{D1}^{(0)} + 2\epsilon_C^{(0)}) \\
E_E^{(1)} &= \epsilon_E^{(1)} + \epsilon_C^{(0)} + \frac{1}{2}(\epsilon_A^{(0)} + \epsilon_B^{(0)} + 2\epsilon_{D1}^{(0)}) \\
E_F^{(1)} &= \epsilon_F^{(1)} + \epsilon_{D1}^{(0)} + \frac{1}{2}(\epsilon_A^{(0)} + 2\epsilon_C^{(0)})
\end{aligned} \tag{22}$$

### *B. Second order calculation and higher orders*

For $n = 2$, the energies of the seven clusters for the twice-inflated tiling can be written out in terms of the energies $\epsilon^{(k)}(z)$ $(k = 0, 1, 2)$. It is easy to obtain the explicit expressions since it suffices to increase all the superscripts in Eq.22 by one (so for example the $\epsilon_i^{(1)}$ become $\epsilon_i^{(2)}$). The zero order energy terms are also easily obtained from the preceding order zero energy terms by use of the proliferation matrix P defined in Eq.8. We give the F cluster energy to this order, as an example:

$$\begin{aligned}
E_F^{(2)} = \epsilon_F^{(2)} + \epsilon_{D1}^{(1)} + \frac{1}{2}(\epsilon_A^{(1)} + 2\epsilon_C^{(1)}) + \\
(\frac{5}{2}\epsilon_A^{(0)} + \epsilon_B^{(0)} + 8\epsilon_C^{(0)} + 6\epsilon_{D1}^{(0)})
\end{aligned} \tag{23}$$

At third order, proceeding similarly, there will be a term in $\epsilon_F^{(3)}$, four terms in $\epsilon^{(2)}$, and a certain number of terms in $\epsilon^{(1)}$ and $\epsilon^{(0)}$. The number of blocks of each type can be found easily using the proliferation matrix to determine the number of ancestors of each type of block. In Fig.11a we have compared the $m_s$ obtained after zero (the dashed curve) with the results at one and two RG steps (open circles and squares). After the second step, the values of $m_s$ converge quickly as can be seen in Fig.11b which shows the third (circles) and fourth order (squares) results along with the QMC data, $m_{loc,s}^{(num)}$.

### *C. Predictions for the full octagonal tiling*

The limiting values of $m_{loc,s}$ are clearly below the QMC data. This is to be expected, due to the bond dilution. One has to correct for the effect of the appreciable bond dilution occurring at C and D sites in order to obtain an estimate of the energy of the undiluted octagonal tiling. On the one hand, the bond dilution leads to having fewer energy terms in the Hamiltonian and consequently underestimating the cluster energies. On the other hand, the loss of bonds is partly offset by the fact that the dilution tends also to suppress frustration and raise the local order parameter. An ad-hoc way to put back the "missing bond-energies" is to add in *half* of the missing link energies at each of the C and D sites. This is easily done here by adjusting the $\tilde{z}$ values at each of the sites, $\tilde{z}_C$ goes up from 5 to 5.5 while $\tilde{z}_{D1}$ is increased from 3 to 4. Using this ad-hoc procedure we can get estimates for $m_s$ values on the original octagonal tiling. The grey squares of Fig.11c were obtained by adjusting the $n = 4$ data in this way. As the figure shows, this procedure yields a fairly good agreement with the QMC data. The same procedure is used to obtain the ground state energy estimate of the full octagonal tiling in the next section.

## 2. Ground state energy

The ground state energy $E_0$ is the sum over all blocks at all orders, of the block energies. At zero order the number of blocks of $z$-spins $N^{(0)}(z) = Nf_i$ ( i.e. proportional to the original frequencies of occurrence given in Eq.1). The density of vertices decreases with each inflation as $\lambda^2$, so that

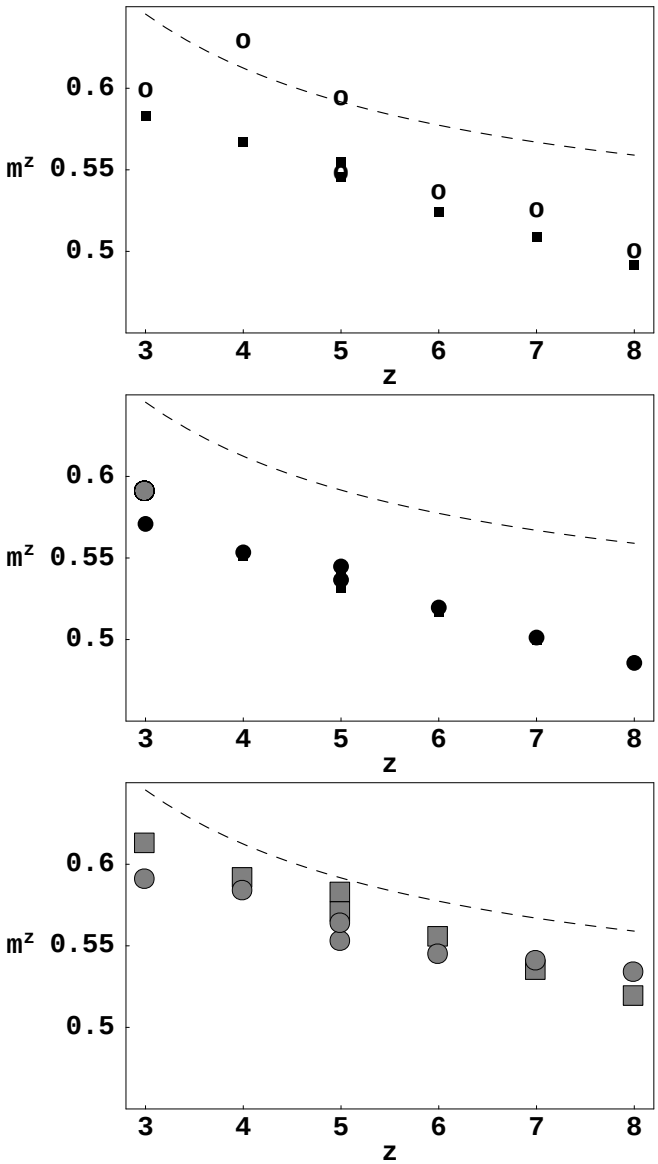


FIG. 11: $m_s(z)$ values versus $z$ obtained for increasing orders of RG. The zero order analytical curve is indicated by a dashed line in each figure. (a) 1st (circles)and 2nd (rectangles) order RG. (b) 3rd (circles) and 4th (rectangles) order RG and QMC data for the full octagonal tiling. (c) Adjusted 4th order data (grey rectangles) and QMC data (grey circles).

$$E_0/N = \sum_{i\in\alpha} f_i(\epsilon_i^{(0)} + \frac{1}{\lambda^2}\epsilon_i^{(1)} + ...\frac{1}{\lambda^{2n}}\epsilon_i^{(n)} + .....) \quad (24)$$

The block energies $\epsilon^{(n)}$ are the energies of blocks with a spin $S_0^{(n)}$ at the center, with effective couplings $\bar{\jmath}^{(n)}$ to the $S_i^{(n)}$ surrounding spins. The series for the energy gives $e_0 \approx -0.51$. We can estimate the effect of bond dilution, as was done for the local order parameters. Using the corrected values of $\tilde{z}$ explained in the last section, one finds an adjusted ground state energy of about $-0.59$. This value of the GS energy is significantly smaller in absolute value than the value deduced from the QMC data in [3]. We recall that this was true of the square lattice calculation as well. In that case, the RG calculation of Delgado and Sierra was already noted in [10] to underestimate the bonding energies of pairs of spins because of the inadequacy of first order perturbation theory around the Neel state. The same is presumably true of our RG on the octagonal tiling. For the former case the RG calculation was compared with the terms of a $1/S$ expansion of the ground state energy, and shown to lack the subleading order term, resulting in the observed discrepancy of values.

On the square lattice, $e_0$ has been determined numerically [25] to high precision to be $-0.6694$, while finite size scaling for the tiling [29] obtains a value of $-0.6581$. The closeness of the values obtained for these two very different problems is rather surprising. It is a probable that this close proximity of values is due to the fact that the octagonal tiling, with its two sublattice structure and its average coordination number of 4. The differences must arise from the next nearest neighbor distributions which differ for the two systems, although this remains to be verified by explicit calculation.

## VI. DISCUSSION AND CONCLUSIONS

In conclusion, we have presented an approximate RG scheme for ground state properties of a two-dimensional quasiperiodic tiling that can be solved after bond dilution. Other approximations involve the truncation of the number of distinct sites and the number of distinct links, and replacing local couplings around sites by average values in order to simplify the effective Hamiltonian after every inflation. The results obtained for the diluted tiling were used to get estimates for the undiluted tiling. Despite these approximations, we believe the model solved is close to the perfect two dimensional quasiperiodic structure, and it allows for a rather detailed solution of real space properties of these heirarchical structures. The results obtained by RG for local order parameters are close to those calculated for the full undiluted model, after our adjustment procedure. It thus appears that the model takes into account the most relevant aspects of the quasiperiodic geometry of the octagonal tiling.

The RG method presented is less good at obtaining the ground state energy, similar to the situation already noted for the square lattice by Sierra and Martin-Delgado, who showed that a better result is obtained by going to second order of perturbation theory to obtain the effective Hamiltonian after renormalization. Concerning the proximity of values of the ground state en-

ergy in these two systems, our calculation is not accurate enough to explain this observation. A calculation to higher order would involve further nearest neighbor sites, improve the energy estimate and perhaps help to explain the small energy difference between the tiling and the square lattice. It would be interesting as well to compare results for other bipartite two dimensional tilings, including the Penrose tiling.

The zero temperature magnetic state of this quasiperiodic Heisenberg antiferromagnet has a structure factor with peaks that can be indexed using the four dimensional indexing scheme (see Appendix). The positions of the peaks is very simply related to the positions of the peaks of the paramagnetic state: they are situated halfway in between. In other words, the paramagnet is indexed by four integers, while the antiferromagnet has half-integer entries, corresponding to the antiferromagnetic vector $\mathbf{q} = \{\frac{1}{2}, \frac{1}{2}, \frac{1}{2}, \frac{1}{2}\}$. This is the quasiperiodic analogue of the square lattice where just such a shift occurs in reciprocal space and corresponds to the antiferromagnetic vector $\mathbf{q} = \{\frac{1}{2}, \frac{1}{2}\}$ (see [30] for a discussion along with a simple one dimensional version of a quasiperiodic antiferromagnet). The real life quasiperiodic compound ZnMgHo was studied by neutron scattering and shown to have short range antiferromagnetic correlations below about 20K. These correlations lead to a magnetic superstructure that is, as for our two dimensional model, shifted with respect to the paramagnetic state. The antiferromagnetic vector that best fits the data has a more complicated value than the simplest form for a 3d quasiperiodic antiferromagnet ($q_i = \frac{1}{2}, i = 1, 6$). This is because the magnetic unit cell is much larger for the three-composant system, due to the fact that only the Ho sites carry a magnetic moment, resulting in smaller spacings between peaks in reciprocal space.

Finally, the RG scheme presented here can be adapted to discuss other discrete quasiperiodic models, such as tight-binding models for electrons hopping between vertices of the tiling. It should provide a useful theoretical framework for describing quasiperiodic tilings in general.

## APPENDIX. THE CUT-AND-PROJECT METHOD.

### 1. One dimensional example

The cut-and-project method of obtaining quasiperiodic tilings is easiest to illustrate in the case of the celebrated one-dimensional tiling – the Fibonacci chain(see Luck's review in [22]). The Fibonacci chain comprises two basic tiles or line segments of two different lengths, "long"(L) and "short"(S) arranged in a deterministic sequence. The Fibonacci chain can be generated iteratively from a single S segment using the following substitution rules: replace each S by an L, and each L by SL. Two successive segments of the infinite chain are shown below to illustrate the substitution rules (dashed lines represent L, thick lines S)

FIG. 12: two segments of the Fibonacci chain

The Fibonacci sequence of segments, or tiles, can be generated by projecting selected edges of a two-dimensional square lattice onto the one dimensional "physical space" $E_1$ as shown in Fig.13. The vertical and horizontal edges project onto the S and the L tiles respectively. The orientation of $E_1$ is given by $\tan^{-1} 1/\tau$ (where $\tau = (\sqrt{5}+1)/2$ is the golden mean, a solution of $\tau^2 - \tau - 1 = 0$), an irrational slope, so the tile sequence never repeats. The edges selected for projection onto $E_1$ obey the following condition: the projection of the edge onto the perpendicular space $E_2$ must fall within the "window of selection" W (indicated by the thick line segment representing the projection of the unit square shown in grey). A finite sequence of twelve edges satisfying this condition are shown in bold in Fig.13 and they result in the projected structure ...LSLLSLLSLSLL...

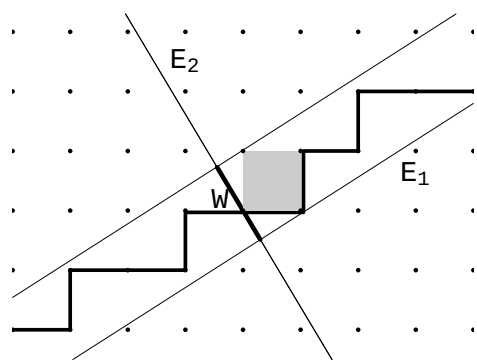


FIG. 13: Cut-and-project method. Selected edges of a square lattice are projected onto the parallel space ($E_1$). The edges that are selected have perpendicular space ($E_2$) projections that fall within the segment marked W.

### 2. Two dimensional case

In analogy with the one dimensional case, the octagonal tiling is obtained from the projection onto $E_{\|}$ (the physical two-dimensional space) of a subset of vertices of a four-dimensional cubic lattice. The subspaces $E_1$,$E_2$

are now two-dimensional, and are invariant under eight-fold rotations in the four dimensional space. The orientation of the physical plane $E_{\|}$ is given by the number $\lambda = 1 + \sqrt{2}$, one of the solutions of $\lambda^2 - 2\lambda - 1 = 0$. The tiles, which are projections in this plane of the 8 faces of the 4d cube, are squares and $45^o$ rhombuses. The vertices (and edges) that are selected for projection in the two dimensional perpendicular space $E_2$ must fall within the window of selection shown in Fig.14. This octagon-shaped area is delimited by the projection of the sides of a four dimensional unit cube. The octagonal tiling has by construction the eight-fold symmetry in the weak sense already described. There are six different kinds of nearest neighbor configurations for vertices of the tiling, denoted A through F as shown in Fig.2.

### *A. Domains of acceptance*

The maximum coordination number $z = 8$ corresponds to the eight-fold symmetric A sites. These sites possess perpendicular space projections that always fall within the central octagon labeled A in Fig.14. Similarly, the projection of all $z = 7$ sites falls within one of the eight triangular regions adjoining the central octagonal domain. The remaining $z$ values likewise correspond to the domains labeled accordingly in Fig.14, which has exact eight-fold symmetry. The ratio of side lengths of similar polygons are either $\lambda$, or $\lambda^2$.

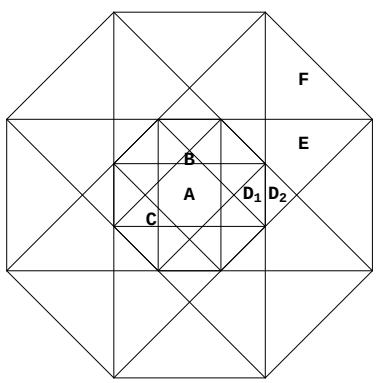


FIG. 14: Projection into perpendicular space of vertices of the octagonal tiling. Domains corresponding to the six families are labeled ( eight-fold symmetry determines labels of unmarked domains)

### *B. Inflations and deflations*

For the octagonal tiling, the inflation transformation is given by a $4 \times 4$ matrix acting in the four dimensional cubic lattice, satisfying $U^2 - 2U - 1 = 0$ and having entries of 0 or 1 only. Projecting the subset of points selected by $u$ leads to a bigger tiling of the same type as the original one. Only the highest $z$ sites remain selected, while the others disappear. The sites that remain are those within the middle octagon, the $\alpha$ family: A, B, C and $D_1$. The sites that disappear correspond to the region outside the middle octagon. The perpendicular space representation also allows to determine rapidly the new $z$ values of the sites that remain: one simply redraws the acceptance domains of Fig.14 after rescaling, inside the middle octagon. Thus a point that was previously in the $D_1$ domain will find itself in the F domain, and the C domains map into E domains. A sites remain A sites if they are close to the center of the diagram, otherwise they become one of the other $\alpha$ sites after inflation. The four categories of A sites mentioned in section II.3 differ by their distance from the origin in perpendicular space. The perpendicular space projection of a site determines its evolution under inflation – the closer a site is to the center of the octagonal selection window, the longer it remains an A site under successive inflations. Also, one clearly sees that D-sites come in two types, with different perpendicular space domains. The following table resumes the old and new site types after inflation:

A $\rightarrow$ A or B or C or $D_1$
B $\rightarrow D_2$
C $\rightarrow$ E
$D_1 \rightarrow$ F

The number of sites per unit area is reduced by the scale factor $\lambda^2$ after each inflation, and the relative frequencies of occurrences of each of the seven families of sites is invariant. The frequency of occurrence of the $i$th family is proportional to the area occupied by that family in the perpendicular space projection. It can thus be easily verified using Fig.14 that these frequencies are: $f_A = \lambda^{-4}; f_B = \lambda^{-5}; f_C = 2\lambda^{-4}; f_{D1} = \lambda^{-3} =; f_E = 2\lambda^{-2}; f_F = \lambda^{-2}$. The average coordination number is exactly 4, as can be checked using the frequencies given. The interested reader can find these and other important geometric and algebraic properties of the system described for example in [23].

### *C. Reciprocal space and structure factor*

The diffraction peaks of the octagonal tiling are found at positions given by projections into 2d of reciprocal lattice vectors $\mathbf{a}_i$ of the 4d cubic structure. The intensities of the peaks are not uniform however, but depend on the Fourier Transform (FT) of the finite selection window. The main features of the diffraction pattern are thus (see Belin et al in [2] for more on the topic)

- The peaks have an eight-fold symmetry around the peak at the origin.

- peaks occur at positions corresponding to the set of integers $h, k, m, n$ representing the projection into the 2d plane of the 4d vector $\mathbf{q} = h\mathbf{a}_1 + k\mathbf{a}_2 + m\mathbf{a}_3 + n\mathbf{a}_4$. That is, one can index peaks by a set of four integers.
- Intensities are highly dependent on the value of $\mathbf{q}$ since the FT of the selction window is oscillatory and long ranged. The set of eight most intense peaks nearest the origin is used to define a quasi Brillouin zone for the tiling.

### *D. Approximants and some of their properties*

Numerical studies of quasiperiodic systems are performed on finite pieces of the infinite system. In particular, it has been pointed out that periodic boundary conditions are preferable to open or closed boundary conditions in terms of eliminating spurious states and eigenvalues. A periodic approximants is a structure that can be periodically continued and can be augmented in size so as approach arbitrarily close to the perfect infinite structure.

This is, again, easiest illustrated by going back to the Fibonacci chain. In the cut and project technique, it should be clear that if one tilts the irrationally oriented selection strip away from the special angle, one will obtain a periodically repeating chain every time the slope is rational.

$\tau^{-1}$ has a series of approximants given in terms of the Fibonacci numbers as follows:$\{\alpha_1, ...\} = \{1, \frac{1}{2}, \frac{2}{3}, \frac{3}{5}, ..., \frac{F_k}{F_{k+1}} ...\}$, where $F_k$ is the $k$th term in the Fibonacci sequence defined by the recurrence relation

$$\begin{aligned} F_{k+1} &= F_k + F_{k-1} \\ F_0 &= F_1 = 1 \end{aligned} \tag{25}$$

with $F_0 = F_1 = 1$. By increasing the value of the denominator of the rational number $F_n/F_{n+1}$ – i.e. by choosing increasingly longer approximants of the golden mean – one will get a structure of period $F_{n+2}$. The finite sequences of L and S within the approximant are the same as those found in an infinitely long chain.

For the two dimensional case, Ref.[27] describes how to obtain square approximants to the octagonal tiling by the projection method. These are obtained from the approximants to the silver mean which depend on ratios of the so-called Octonacci sequence : $\lambda_k = O_{k+1}/O_k$ where

$$\begin{aligned} O_{k+1} &= 2O_k + O_{k-1} \\ O_1 &= 1; \qquad O_2 = 2 \end{aligned} \tag{26}$$

with $O_1 = 1; O_2 = 2$. These are the finite size systems used for a number of numerical studies including the quantum Monte Carlo calculations. The first few square approximants have the following sizes

| k | 2 | 3 | 4 | 5 |
|---|---|---|---|---|
| $N_k$ | 239 | 1393 | 8119 | 47321 |

Table A.1. Number of sites in the first four square approximants

We will list some features of these approximants that may be important to bear in mind depending on the models studied.

- Reflection symmetry (exact) with respect to the bottom left-top right diagonal
- $90^o$ Rotation symmetry around the center (approximate)
- Odd parity of repetition. By this is meant that one changes sublattice when one goes from a site to its first periodic repetition along either x or y directions. For a number of numerical calculations it is easiest to restore the bipartite property by taking a system size doubled along both directions (i.e. quadrupled unit cell with respect to the sizes given in the Table).
- Inflation relation between approximants. Fig.15 shows a small approximant superimposed on the next largest one.

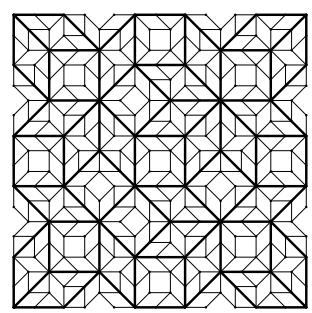

FIG. 15: Superposition of two successive approximants


[1] T. J. Sato, H. Takakura, A. P. Tsai, K. Shibata, K. Ohoyama, and K. H. Andersen, Phys. Rev. B **61**, 476 (2000)

[2] E. Belin-Ferre et al, Eds.*Quasicrystals. Current Topics*, World Scientific, 2000

[3] S. Wessel et al, Phys.Rev.Lett. **90** 177205 (2003)

[4] Joachim Hermisson, J. Phys. A**33** 57 (2000); J. Hermisson, U. Grimm and M. Baake, J. Phys. A**30** 7315 (1997)

[5] Kazuo Hida, J.Phys.Soc.Jpn, **68** 3177 (1999); P.R.L. **86** 1331 (2001); Phys. Rev. Lett. **93** 037205 (2004)

[6] J. Vidal et al, Phys. Rev. Lett. **83** 3908 (1999); Phys. Rev. B **65** 014201 (2001)

[7] C. Godreche, J. M. Luck, and H. Orland, J. Stat. Phys. **45**, 777 (1986).

[8] Vedmedenko, Phys.Rev.Lett. **90** 137203 (2003)

[9] A. Jagannathan and H.J.Schulz, Phys. Rev. B **?**

[10] Miguel A. Martin-Delgado, in *Strongly Correlated Magnetic and Superconducting Systems*, Springer Lecture Notes in Physics, **478** (1996); G. Sierra and M.A.Martin-Delgado, Phys.Lett. **391B** 381 (1997)

[11] A. Jagannathan, Phys.Rev.Lett. **92** 047202 (2004)

[12] J. E. S. Socolar, Phys. Rev. B **39** 10519 (1989)

[13] C. Sire and J. Bellissard, Eur. Lett. **11** 439 (1990), V.G. Benza and C.Sire, Phys. Rev. B **44** 10343 (1991), F.Piechon and AJ, Phys. Rev. B **51** 179 (1995), AJ in J. Phys. I (France)**4** 133 (1994)

[14] Sire and Benza, E.S. Zijlstra, Phys. Rev. B **66** 214202 (2002)

[15] T. Janssen, J. Los and F. Gaehler, Intl. J. Mod. Phys. **7** 1505 (1993)

[16] R. Penrose, Math Intelligencer,**2** 32 (1979)

[17] M. Gardner, *Scientific American*, p.110 (Jan.1977)

[18] P. J. Steinhard and S. Ostlund, The physics of Quasicrystals, World Scientific 1987

[19] M. Duneau and A. Katz, Phys. Rev. Lett. **54** 2688 (1985); P. Kalugin, A.Y. Kitaev and L.S. Levitov, JETP Lett. 41 145 (1985); V. Elser, Acta Cryst. **42** 36 (1986)

[20] C. L. Henley in Quasicrystals: The State of the Art, Eds. P.J. Steinhardt and D.P. Di Vincenzo, World Scientific (1991)

[21] J.X.Zhong and R. Mosseri, J. Phys. I (France) **4** 1513 (1994)

[22] J.M. Luck, Fundamental Problems in Statistical Mechanics VIII (Elsevier 1993)

[23] Michel Duneau and D. Gratias in Marrakech school

[24] The two kinds of D-site also can be distinguished in real space by counting the number of second nearest neighbors.

[25] A. Sandvik, Phys. Rev. B **66** 024418 (2002)

[26] Fractals and Disordered Systems, Eds. A. Bunde and S. Havlin, Springer-Verlag (Berlin 1991)

[27] Michel Duneau, Remy Mosseri and Christophe Oguey, J. Phys. A **22** 4549 (1989)

[28] Note a slight change of definition of $m_s$ from that of ref.3.

[29] S. Wessel, private communication

[30] Ron Lifshitz, Mat. Sci. Engg bf 294 508 (2000)